Near-UV Sources in the Hubble Ultra Deep Field: The Catalog

Elysse N. Voyer[1,2], Duilia F. de Mello[1,3]

Catholic University of America Washington, DC 20064

Brian Siana

California Institute of Technology, MS 105-24, Pasadena, CA 91125

Jonathan P. Gardner

Observational Cosmology Laboratory, Goddard Space Flight Center, Code 665, Greenbelt, MD 20771

Cori Quirk

Catholic University of America Washington, DC 20064

and

Harry I. Teplitz

Spitzer Science Center, California Institute of Technology, MS 220-6, Pasadena, CA 91125

Received _____; accepted _____

[1]Observational Cosmology Laboratory, Goddard Space Flight Center, Code 665, Greenbelt, MD 20771

[2]NASA Graduate Student Research Program Fellow

[3]Visiting Scientist in the Department of Physics and Astronomy, Johns Hopkins University, Baltimore, MD 21218

ABSTRACT

The catalog from the first high resolution U-band image of the Hubble Ultra Deep Field, taken with Hubble's Wide Field Planetary Camera 2 through the F300W filter, is presented. We detect 96 U-band objects and compare and combine this catalog with a Great Observatories Origins Deep Survey (GOODS) B-selected catalog that provides B, V, i, and z photometry, spectral types, and photometric redshifts. We have also obtained Far-Ultraviolet (FUV, 1614 Å) data with Hubble's Advanced Camera for Surveys Solar Blind Channel (ACS/SBC) and with Galaxy Evolution Explorer (GALEX). We detected 31 sources with ACS/SBC, 28 with GALEX/FUV, and 45 with GALEX/NUV. The methods of observations, image processing, object identification, catalog preparation, and catalog matching are presented.

Subject headings: galaxies:evolution-galaxies:formation-galaxies:starburst

1. Introduction

The Hubble Ultra Deep Field (UDF) campaign (Beckwith et al. 2006) has produced the deepest optical images of our universe to date. The UDF was observed by Hubble in 412 orbits that were centered in a region of the Chandra Deep Field South (CDF-S) which was also the target of the Great Observatories Origins Deep Survey (GOODS, Giavalisco et al. 2004) known as the GOODS south or GOODS-S. The UDF used the same Advanced Camera for Surveys (ACS) filters as GOODS, F435W (B_{435}), F606W (V_{606}), F775W (i_{775}), and F850LP (z_{850}), but covered only one field of the 15 GOODS-S fields. The UDF reached approximately uniform limiting magnitudes $m_{AB}\sim 29$ for point sources, at least two magnitudes deeper than GOODS. Both campaigns, the UDF and GOODS, did not include deep imaging in the U bandpass. Taking U-band photometry is a time consuming task because longer integrations are required to achieve comparable depth to optical images. Only three HST U-band deep fields have been taken so far, the original Hubble Deep Field, the Hubble Deep Field South and the deepest U-band ever taken with Hubble which was part of the parallel campaign of the UDF and lies on the edge of the GOODS-S (Williams et al. 1996, Casertano et al. 2000, de Mello et al. 2006b). GOODS has only partial U-band coverage with HST obtained during parallel observations (de Mello et al. 2006a). Deep U-band ground-based images of the GOODS-S field, such as those taken with the CTIO 4m and ESO 2.2m available in the GOODS webpage[5], are included in the multiwavelength coverage of GOODS. Although ground-based observations can cover larger fields of view than Hubble's cameras more efficiently, they do not possess the same angular resolution as space-based observations. Low-resolution ground-based images will blend together nearby detections leading to inaccurate photometric redshifts and morphological analysis. The U-band is a critical wavelength in studies at intermediate redshifts ($z < 2$) since the

[5]http://www.stsci.edu/science/goods/SupportObs/cdfs_mosaic/

rest-frame UV light is redshifted into the U bandpass. It is in the UV that short-lived, massive, O and B stars radiate most of their energy and therefore the U-band is necessary to probe the unobscured star-formation activity in galaxies at z < 2.

After a redshift of z∼1.5-2, the star-formation rate of the universe began to steadily decline, decreasing by more than an order of magnitude (e.g. Hopkins & Beacom 2006, Wadadekar, Casertano & de Mello 2006). However, it is still an open question as to what population of objects contributes to the SFR density during the decline, and whether downsizing (the shift in star-formation being dominated from large to small mass galaxies as the universe aged) plays an important role in this era (Cowie et al. 1996, Savaglio et al. 2005, Mouri and Taniguchi 2006, Neistein, van den Bosch, & Dekel 2006). Therefore, studies that use U-band observations to better understand the nature of star-forming galaxies at intermediate-z can greatly contribute to connecting the early universe and the local universe.

In this paper we present the first HST targeted U-band image of the UDF. We present the U-band object catalog, and describe the methods used for observations, image processing, object identification, and catalog preparation.

2. Observations

The U-band observations were obtained with the HST Wide Field Planetary Camera 2 (WFPC2) in the Cycle 13 HST Treasury proposal (Teplitz, Program 10403). The UDF was imaged in the near UV (NUV) through the WFPC2/F300W filter ($\lambda_{\rm max}$ = 2987Å, $\Delta\lambda$=740Å) in 12 HST orbits divided into 4 roll angles to compensate for the shape of the WFPC2 chevron and achieve uniform depth. On-chip binning (2x2) was applied during WFPC2 observations to reduce the effects of read-out noise, i.e. each Wide Field became

400 × 400 pixels. A total of 24 WFPC2 images were taken with individual exposure times of 1200s.

FUV imaging was also obtained in this proposal with HST/ACS Solar Blind Channel (SBC) camera at which time WFPC2 parallel observations were also made. The UDF ACS/SBC images were taken in 50 HST orbits using the long-pass quartz filter (F150LP) ($\lambda_{\rm eff}$ = 1614Å, and FWHM=177Å). The FUV was imaged in 25 pointings. Each pointing had a four point dither pattern with two 650s exposures at each dither position. The total exposure time per pointing was ∼5200s (Siana et al. 2007).

3. Image Processing

The WFPC2 images were retrieved from the HST archive for further processing. We combined the 24 WFPC2 images with the MultiDrizzle code in the PyDrizzle package (Koekemoer et al. 2002). These images were taken using a dithering technique that reduces effects of pixel-to-pixel errors and allows one to better remove hot pixels, bad columns, and charge traps from the image. Dithering also allows the recovery of information lost to undersampling by pixels that are not small compared to the point spread function (PSF). MultiDrizzle simplifies and automates the detection of cosmic-rays of these dithered observations. We used calibrated flat-fields from the HST pipeline and ran the MultiDrizzle script through the following steps. First, a static mask was created to identify bad pixels, then each image was sky-subtracted, shifts were determined from header coordinates for each image and were applied in drizzling each image separately onto registered output images. Next, a median image was created from these separate drizzled images and was blotted back to each original input image. Finally, the blotted images were used to compute cosmic ray masks, and the final drizzle combination was performed using these masks.

Prior to running MultiDrizzle the Planetary Camera (PC) data was removed from all images because its inclusion greatly increased the noise level of the output drizzled image. This was achieved by replacing the PC in each of the 24 images with hot pixels, forcing MultiDrizzle to automatically include the PC in the pixel mask for each individual image. We set the user-inputs to MultiDrizzle so the script would output separate science and weight images for these data that we have made available online at: http://goods.gsfc.nasa.gov/release/UDF_F300W.

The drizzled WFPC2 image shown in Figure **??** has a total exposure time of 28,800s and a pixel scale of 0.1 arcsec. Due to the nature in which the 24 WFPC2 pointings were positioned, the final drizzled image does not have of a uniform depth. The majority of pointings overlap in the mid-upper region of the combined image. Consequently, the majority of UV sources are detected in this area of the UDF. Also, the upper-most section of the U-band image lies just outside the UDF footprint, and sources from this area are marked as such in the catalog. The reduction procedure used for the UDF ACS/SBC images is outlined in Teplitz et al. (2006).

4. Object Identification And Catalog Preparation

The catalog of U-band sources was produced using SourceExtractor version 2.5 (Bertin & Arnouts 1996, hereafter SE). Initially, we created both a low-σ (1.5σ above background noise) and a high-σ (3σ above background noise) catalog. The high-σ catalog contains all visually confirmed sources in the image, while the low-σ catalog may contain spurious detection. The difference between the SE parameters specified for these two catalogs was the detection threshold relative to the background RMS. For both catalogs, the minimum area of adjoining pixels for a detection was 15 pixels, and the minimum deblending parameter was set at 10%, except for a few cases where we set the deblending value in order to avoid

multiple detections in one single object. This is particularly critical for source detection in U-band images since star-forming regions can appear as multiple clumps in one object. SE might detect those clumps as individual objects making false identifications.

The GAIN, MAG_ZEROPOINT, and SATUR_LEVEL parameters which are specific to the WFPC2 camera were set to 7 e^-/ADU, 20.77 mag, and 2 ADU/s, respectively. The weight map produced by the drizzling process was used by setting the weight map type to MAP_WEIGHT. Photometric measurements of each source were calculated using SE's automatic aperture magnitudes (MAG_AUTO). MAG_AUTO uses a Kron (1980) flexible elliptical aperture to measure the total magnitude of each source. Instead of using the classical aperture photomery with a fixed aperture radius, MAG_AUTO has the advantage of limiting the background noise while detecting light from faint sources more effectively. The size of the background mesh which is subtracted from the photometry of each source (BACK_SIZE) was set to 64 pixels, and its RMS value is used to calculate photometric errors. We cleaned the high-σ and low-σ catalogs removing sources with photometric errors ≥ 1.0.

The resulting U-band catalog includes all detections from the high-σ catalog, and the remaining objects visually confirmed from the low-σ catalog. The U-band 1.5σ limiting magnitude measured within a $1''$ diameter aperture is 23.5mag (AB) (Figure **??**).

4.1. Visual Identification Of U-Band Sources

We have visually checked each SE U-band detection in order to decide (i) if a single source detection is actually multiple sources, (ii) if multiple source detections are single sources, (iii) if a detection is too noisy, or (iv) if there are any faint UV sources which are not detected. When such cases occur, SE parameters can be adjusted to maximize U-band

source detections in the UDF image, and non-detections can be omitted from the catalog.

We have also visually identified the U-band sources within a Hubble ACS/B-band image of the GOODS-S field that overlaps the UDF. The B-band sources had been cataloged by the GOODS team using SE and have matched aperture photometry in multiple ACS bands (V,i,z) (Dahlen et al. 2007). The B-band catalog also lists spectral types (see §5 for definition) and photometric redshifts with a typical GOODS accuracy of Δ_z=0.8 (where $\Delta_z \equiv \langle |z_{phot}\text{-}z_{spec}|/(1+z_{spec}) \rangle$) (Dahlen et al. 2007) for each source. If a U-band detection could not be visually identified as one of the objects in the B-band catalog it was removed from the U-band catalog. We did this because the B-band data is much deeper (limiting 10σ sensativity is 27.8; Giavalisco et al. 2004) than the U-band, and we would not expect to detect a source in the U-band without also seeing it in the B-band. During this cleaning the majority of spurious U-band detections located in the borders of the WFPC2 image were removed. We also discovered five B-band objects that corresponded to multiple detections in the U-band. This was a result of setting SE's deblending parameters to a low value in an effort to detect as many U-band sources as possible. This parameter was adjusted in an additional SE run to obtain single detections of these sources. The final U-band catalog contains 96 objects.

4.2. Catalog Matching

We matched the final U-band catalog to a far-UV (ACS/SBC) catalog of the UDF area (Siana et al. 2007). Each ACS/SBC source was matched to the nearest U-band object within a 2.5″ radius. Thirteen U-band sources do not have FUV detections because they are outside the ACS/SBC footprint. Any ACS/SBC sources with signal to noise $< 3\sigma$ were not considered. In total, 31 of the 96 U-band objects have resolved matching ACS/SBC detections.

The UDF has also been observed with the Galaxy Evolution Explorer (GALEX) mission in the far and near ultraviolet (FUV: $\lambda_{\rm eff}$=1528Å $\Delta\lambda_{FUV}$=269Å NUV: $\lambda_{\rm eff}$=2271Å $\Delta\lambda_{NUV}$=616Å; GALEX field of view is 1°.28 and 1°.24 in FUV and NUV, and pixel scale is 1.5″/pixel) and is publicly available in the GALEX Release 4 (GR4) at the Multimission Archive at STScI (MAST). These data are from two different surveys, the All Sky Survey (AIS, 4″.3 FWHM) and the Deep Sky Survey (DIS, 5″.3 FWHM). The 5σ limiting magnitudes of the AIS data are 20.8 in the NUV and 19.9 in the FUV, and for the DIS data 24.4 in the NUV and 24.8 in the FUV (Morrissey et al. 2007).

We searched for all U-band objects in the GR4 and found 28 detected by GALEX/FUV and 45 in the NUV. Since GALEX resolution is significantly lower than Hubble's (GOODS ACS image has 0.03″/pixel) we have searched for objects where confusion might be problematic and one should use the GALEX data with caution. We found 22 objects where confusion was an important factor in the NUV and FUV and have flagged them in the catalog. In Figure **??** we show an example of a single GALEX NUV detection of at least four identified objects in the U and B-band.

5. The Catalog

Table 1 presents the U-band catalog of the UDF NUV sources. Columns (1) and (2) are the GOODS World Coordinate System (WCS) Right Ascension and Declination in degrees. Three objects with Chandra X-ray detections (Koekemoer et al. 2004) are flagged as "a" [1]. Columns (3)-(8) are the U, FUV, B, V, i, and z magnitudes and photometric errors (MAG_AUTO), respectively. The B, V, i, and z magnitudes were obtained from the

[1]Seven other Chandra X-ray sources found in the UDF were not detected in our U-band image.

GOODS-S B-selected catalog. Note that not all U-band detections have FUV photometry because they are either outside the ACS/SBC footprint, are non-detections (S/N $< 3\sigma$), or are not resolved in the FUV imaging. Columns (9) and (10) are GALEX NUV and FUV magnitudes from the GR4. Sources with confusion are flagged as "c" in column 1. Columns (11) and (12) list photometric redshifts (z_{phot}) for all objects, and available spectroscopic redshifts (z_{spec}) for 21 objects. The z_{spec} are from the GOODS collaboration (taken from the ESO/GOODS-S spectroscopy masters catalog[6]), and Figure **??** plots z_{spec} as a function of z_{phot} for these objects. Column (14) are spectral types from the GOODS B-selected catalog based on spectral energy distributions from Coleman et al. (1980) and Kinney et al. (1996). The U-band catalog, including U, FUV, B, and BVi postage stamp images of each source, is available online at: http://goods.gsfc.nasa.gov/release/UDF_F300W /original/gallery/udf_u_fuv.html.

We are grateful to the GOODS team. Support for this work was provided by NASA through grants HST-GO-10403.13A and HST-GO-10632.03A from the Space Telescope Science Institute, which is operated by the Association of Universities for Research in Astronomy, Inc., under NASA contract NAS5-26555. DFdM and E.V. were funded by NASA Research Grants NNG05GG06G and NNX08AR95H. We are grateful to Ms. Sara Petty for helping with the early stages of this project.

GALEX is a NASA Small Explorer, launched in 2003 April. We gratefully acknowledge NASA's support for construction, operation, and science analysis for the GALEX mission, developed in cooperation with the Centre National d'Etudes Spatiales of France and the Korean Ministry of Science and Technology.

[6]See http://www.eso.org/science/goods/spectroscopy/CDFS_Mastercat.

REFERENCES

Bertin, E., & Arnouts, S. 1996, A&AS, 117, 393

Casertano, S., et. al. 2000, AJ, 120, 2747

Coleman, G.D., Wu, C-C., & Wedman, D.W. 1980, ApJS, 43, 393

Cowie, L.L., Songalia, A., Hu, E.M., & Cohen, J.G. 1996, AJ, 112, 839

Dahlen, T., Mobasher, B., Dickinson, M., Ferguson, H.C., Giavalisoc,M., Kretchmer, C., & Ravindranath, S. 2007, ApJ, 654, 172D

de Mello, D.F., Dahlen, T., Gardner, J.P., & Grogin, N.A. 2006a, AJ, 132, 2014

de Mello, D.F., Wadadekar, Y., Dahlen, T., Casertano, S., & Gardner, J.P. 2006b, AJ, 131, 216

Giavalisco, M., et al. 2004, ApJ, 600, L93

Hopkins, A.M., & Beacom, J.F. 2006, ApJ, 651, 142

Kinney, A., Calzetti, D., Bohlin, R.C., McQuade, K., Storchi-Bergmann, T., & Schmitt, H. 1996, ApJ, 467, 38

Koekemoer, A. M., Fruchter, A. S., Hook, R. N., Hack, W. 2002, HSTC Conf., 337K

Koekemoer, A. M., et al. 2004, ApJ, 600, L123

Kron, R.G. 1980, ApJS, 43, 305

Morrissey, P., et al. 2007, ApJS, 173, 682

Mouri, H., & Taniguchi, Y. 2006, A&A, 459, 371

Neistein, E., van den Bosch, F.C., & Dekel, A. 2006, MNRAS, 372, 933

Savaglio, S., et al. 2005, ApJ, 635, 260S

Siana, B., et al. 2007, ApJ, 668, 62S

Teplitz, H.I., et al. 2006, AJ, 132, 853

Wadadekar, Y., Casertano, S., & de Mello, D.F. 2006, AJ, 132, 1023

Williams, R. et al. 1996, AJ, 112, 1335

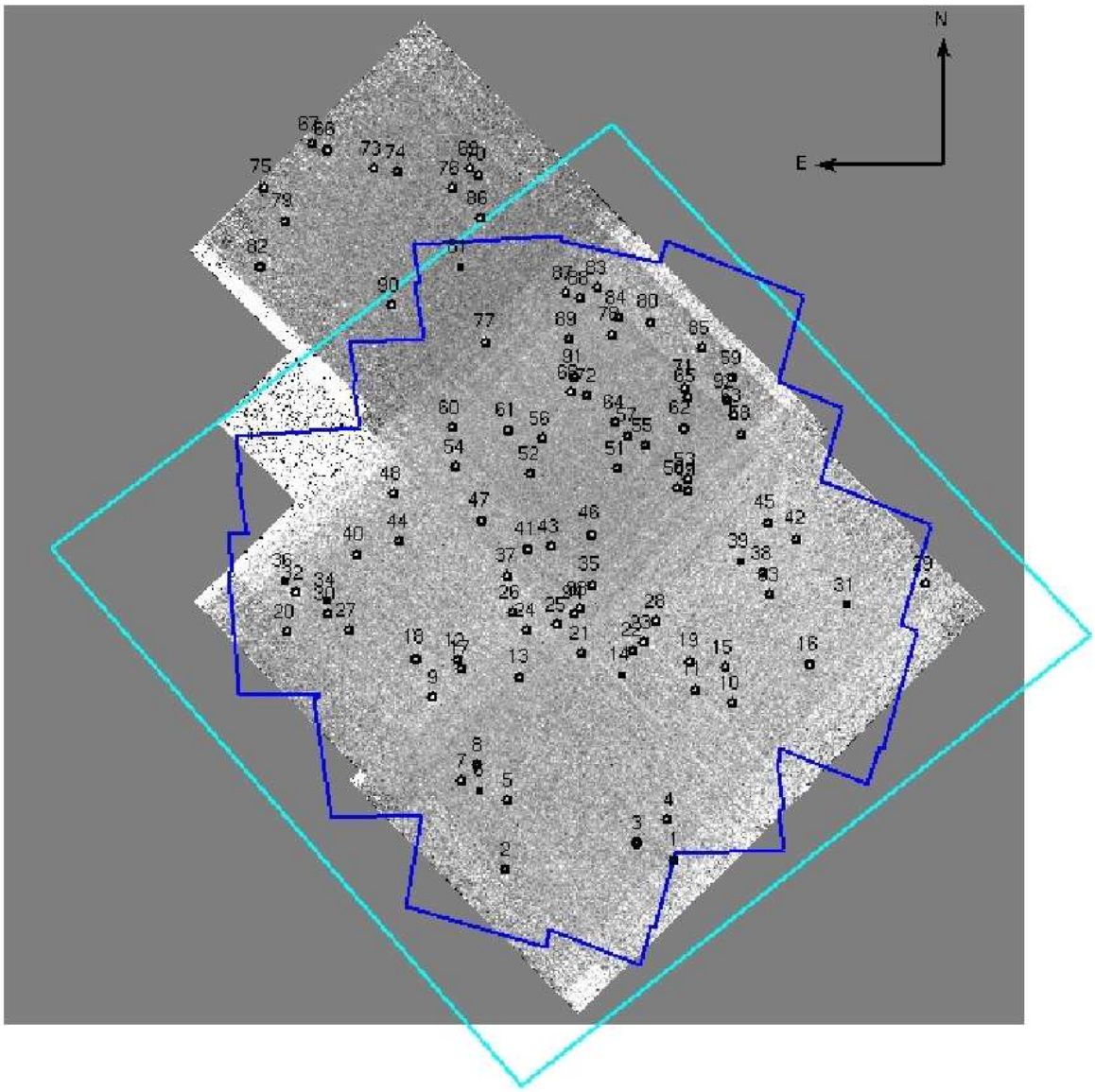

Fig. 1.— WFPC2 drizzled U-band image overlayed with UDF(cyan) and ACS/SBC(blue) footprints. Note the large number of detections in the second rectangular region from the top of the image due to a higher net exposure time for this region.

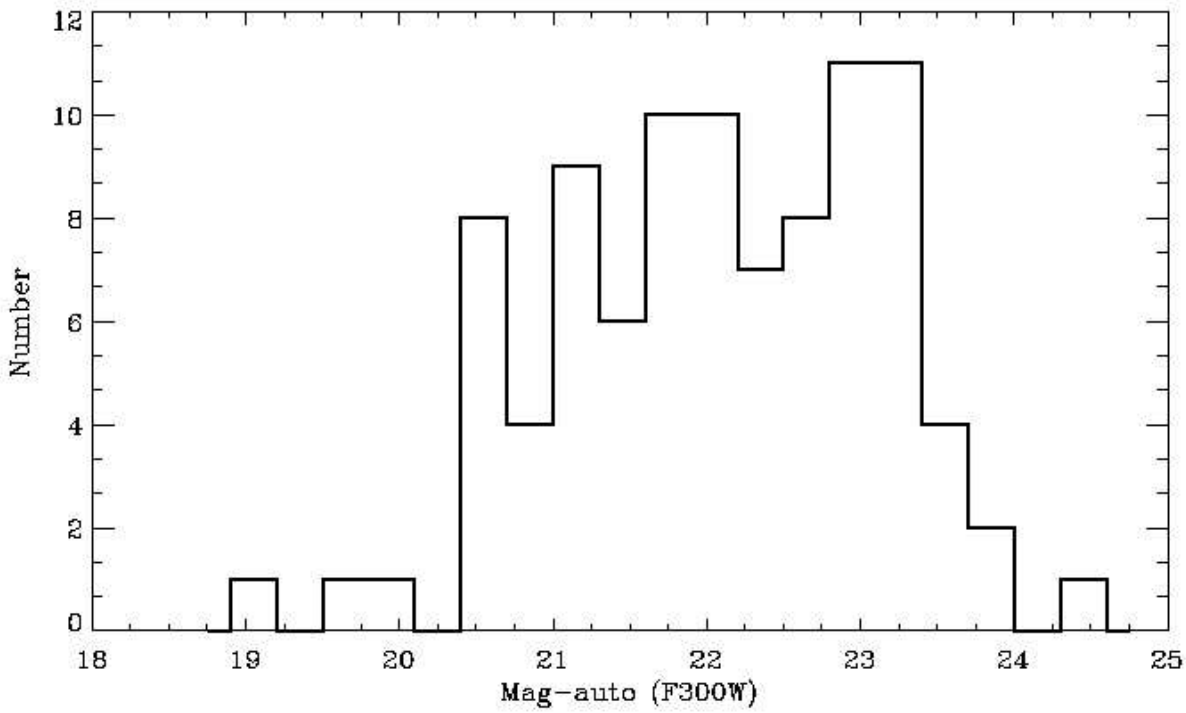

Fig. 2.— Magnitude distribution of the U-band catalog, MAG_AUTO from SE.

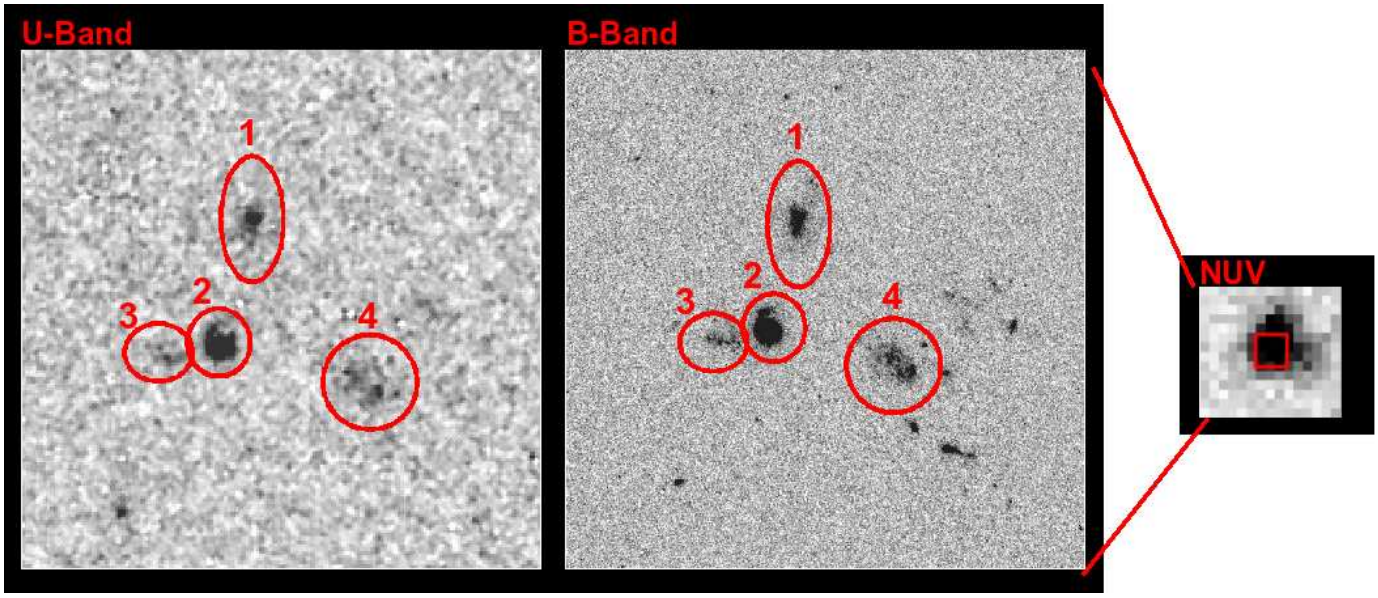

Fig. 3.— WFPC2 (left), ACS (center), and GALEX (right) images showing four objects (1: 53.1619949 -27.7739410, 2: 53.1623802 -27.7750893, 3: below magnitude limit of the U-band catalog, 4: 53.1608238 -27.7753963) which are within the GALEX beam. All three images are $20'' \times 20''$.

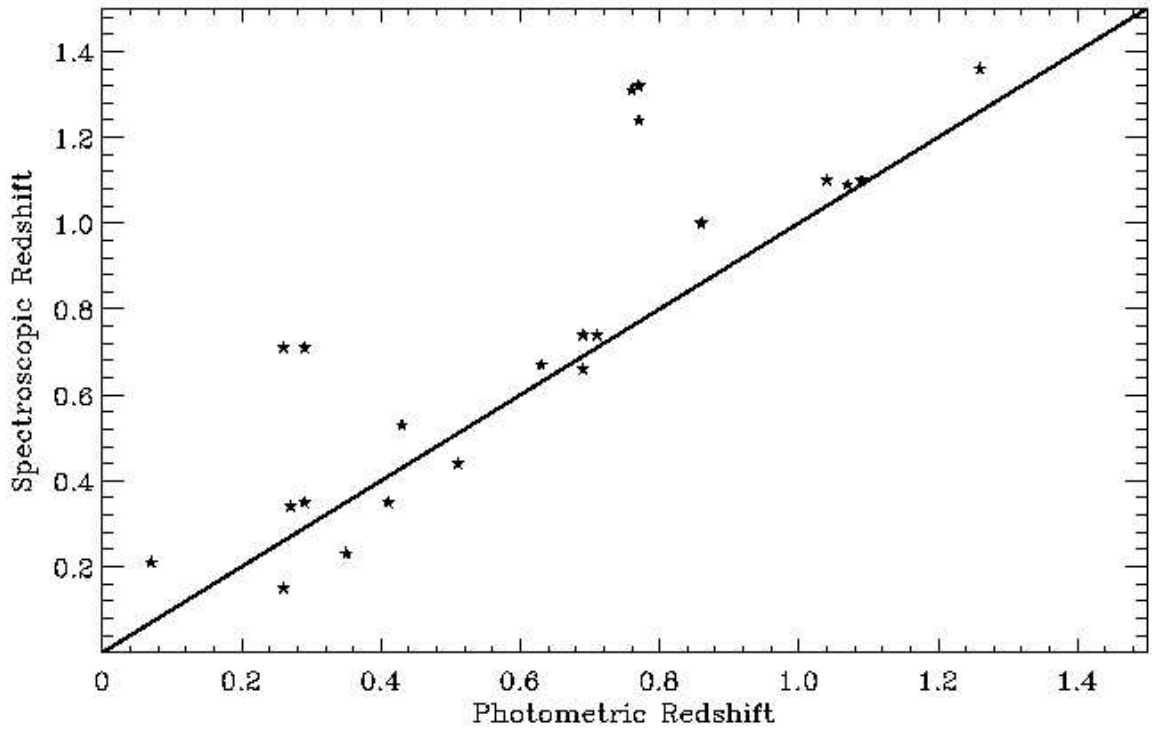

Fig. 4.— Photometric Redshifts from GOODS vs. Spectroscopic Redshifts from the ESO/GOODS Chandra Deep Field-South spectroscopy masters catalog.

Table 1. UDF U-band Sources

RA (Deg)	Dec (Deg)	U_{mag}	FUV_{mag}	B_{mag}	V_{mag}	i_{mag}	z_{mag}	GALEX NUV_{mag}	GALEX FUV_{mag}	z_{phot}	z_{spec}	ST
53.1306038	-27.7902641	20.50±0.05	...	22.46±0.02	21.80±0.01	21.16±0.01	21.01±0.01	23.52±0.07	25.69±0.25	0.66	...	3.67
53.1376457	-27.7919559	21.70±0.07	...	23.54±0.04	23.13±0.02	22.44±0.03	22.04±0.02	...	...	0.85	...	3.67
53.1409721	-27.7966537	22.12±0.05	24.97±0.06	23.54±0.04	22.47±0.01	21.95±0.02	21.69±0.02	24.63±0.24	...	0.41	0.3500	3.00
53.1421356	-27.7866974	21.02±0.03	23.55±0.03	22.11±0.01	21.15±0.01	20.73±0.01	20.57±0.01	23.18±0.09	23.90±0.16	0.35	0.2262	3.33
53.1445389	-27.7911339	21.58±0.06	...	24.22±0.07	24.16±0.05	24.04±0.09	23.84±0.09	...	...	1.80	...	6.00
53.1447334	-27.7854404	20.97±0.03	23.82±0.04	23.20±0.02	22.58±0.01	22.47±0.02	22.51±0.02	23.44±0.07	23.78±0.08	0.07	...	6.00
53.1450996	-27.7894268	23.19±0.11	...	24.15±0.06	23.96±0.04	23.58±0.06	23.07±0.05	...	...	0.84	...	5.33
53.1470947[c]	-27.7784290	22.46±0.08	...	24.43±0.06	24.28±0.04	23.93±0.06	23.73±0.06	24.91±0.25	...	1.12	...	6.00
53.1472054	-27.7884884	22.71±0.08	26.29±0.16	24.52±0.06	23.99±0.03	23.35±0.04	23.19±0.04	...	...	0.73	...	4.00
53.1477814	-27.7769451	21.87±0.07	...	24.74±0.06	24.66±0.05	23.90±0.05	23.43±0.04	...	...	1.07	1.0860	3.67
53.1478577[c]	-27.7740345	20.58±0.03	...	22.59±0.02	22.33±0.01	21.76±0.02	21.30±0.01	23.03±0.07	...	1.02	...	4.00
53.1479225	-27.7996845	23.00±0.10	26.13±0.09	25.06±0.15	24.35±0.07	23.75±0.08	23.58±0.08	...	...	0.67	...	4.00
53.1484451	-27.7757874	22.80±0.07	25.56±0.09	24.14±0.04	23.24±0.02	22.68±0.02	22.45±0.02	22.75±0.10	...	0.48	3.6664	3.33
53.1485405	-27.7968845	22.48±0.08	...	23.56±0.03	23.52±0.03	23.49±0.05	23.43±0.05	...	...	1.84	...	6.00
53.1506119	-27.7715912	20.51±0.04	22.73±0.02	22.24±0.02	21.54±0.01	21.26±0.01	21.19±0.01	22.62±0.07	22.93±0.09	0.23	...	4.67
53.1512375	-27.7986679	21.51±0.06	25.86±0.09	24.93±0.08	24.37±0.04	23.64±0.04	23.83±0.06	...	...	0.47	...	6.00
53.1516838	-27.7964039	22.93±0.11	...	23.77±0.04	23.49±0.03	23.35±0.05	23.15±0.05	...	...	1.56	...	5.67
53.1518784[c]	-27.7754364	21.97±0.05	...	23.76±0.05	23.36±0.03	22.58±0.03	22.17±0.02	22.93±0.06	...	1.00	...	3.33
53.1518898[c]	-27.7828751	22.73±0.04	...	24.44±0.04	24.14±0.03	23.45±0.03	23.23±0.03	24.11±0.13	...	0.71	...	4.00
53.1518974[c]	-27.7819862	23.17±0.08	...	24.60±0.06	24.32±0.04	23.72±0.05	23.32±0.04	24.19±0.18	...	0.84	...	4.00
53.1520653[c]	-27.7747822	21.65±0.03	...	22.64±0.02	22.15±0.01	21.37±0.01	21.16±0.01	22.93±0.06	...	0.70	...	3.67
53.1523628[c]	-27.7779751	22.99±0.06	...	24.71±0.08	24.84±0.07	24.96±0.16	24.29±0.10	22.93±0.06	...	1.55	...	6.00
53.1528244[c]	-27.7826958	23.57±0.06	28.01±0.26	25.52±0.10	25.21±0.07	24.61±0.09	24.25±0.08	24.11±0.13	...	0.70	...	6.00

Table 1—Continued

RA (Deg)	Dec (Deg)	U_{mag}	FUV_{mag}	B_{mag}	V_{mag}	i_{mag}	z_{mag}	GALEX NUV_{mag}	GALEX FUV_{mag}	z_{phot}	z_{spec}	ST
53.1531296	-27.8120804	21.04±0.04	...	23.85±0.04	23.38±0.02	23.30±0.04	23.33±0.05	24.11±0.12	24.21±0.10	0.07	0.2128	6.00
53.1536751	-27.8089409	22.06±0.06	25.89±0.14	24.92±0.08	24.12±0.03	23.80±0.05	23.62±0.05	...	...	0.29	...	5.33
53.1546783	-27.7932301	21.29±0.04	23.86±0.03	23.44±0.02	22.86±0.01	22.65±0.02	22.62±0.02	23.18±0.09	23.79±0.09	0.41	...	6.00
53.1552696	-27.7695465	21.67±0.06	...	23.65±0.05	23.07±0.02	22.38±0.03	22.13±0.03	...	...	0.71	0.7359	3.67
53.1556816	-27.7793083	23.96±0.09	...	23.99±0.05	23.68±0.03	23.28±0.04	23.16±0.04	...	...	1.58	...	4.00
53.1559105[c]	-27.7948895	21.82±0.08	...	24.02±0.04	23.79±0.03	23.43±0.05	23.11±0.04	24.63±0.12	...	0.91	...	5.67
53.1564293	-27.8107758	20.45±0.02	24.69±0.09	22.20±0.02	21.62±0.01	20.97±0.01	20.84±0.01	22.90±0.08	...	0.63	0.6650	3.67
53.1567726[c]	-27.7955532	22.17±0.07	...	23.79±0.04	23.31±0.02	22.66±0.03	22.08±0.02	23.34±0.15	...	1.09	1.0970	3.33
53.1572227	-27.7785568	22.78±0.06	...	24.59±0.05	24.53±0.04	24.41±0.07	23.83±0.05	...	...	0.76	1.3070	6.00
53.1578369	-27.7974815	22.27±0.10	...	23.62±0.03	23.26±0.02	22.61±0.03	22.40±0.03	23.34±0.15	...	0.70	...	4.00
53.1580658	-27.7692299	21.92±0.02	...	21.18±0.01	20.40±0.00	20.02±0.01	19.91±0.00	23.79±0.14	...	0.11	...	3.00
53.1581879	-27.7811279	21.00±0.02	24.10±0.04	22.93±0.02	22.43±0.01	21.93±0.02	21.90±0.02	23.22±0.09	25.13±0.34	0.44	...	5.67
53.1583176	-27.7774792	22.76±0.04	...	24.77±0.06	24.79±0.05	24.75±0.09	24.64±0.10	...	...	1.88	...	6.00
53.1587791	-27.7705669	22.47±0.04	...	23.90±0.04	23.56±0.03	22.84±0.03	22.45±0.02	23.86±0.22	...	0.91	...	3.67
53.1599007	-27.7668762	23.39±0.27	...	24.76±0.07	24.72±0.06	24.02±0.07	23.59±0.06	21.86±0.04	...	0.90	...	4.00
53.1604424	-27.7903595	23.03±0.07	...	24.01±0.04	24.01±0.03	23.92±0.05	23.92±0.06	...	...	1.82	...	6.00
53.1604996	-27.7863064	23.83±0.07	...	25.50±0.15	25.36±0.11	24.55±0.11	24.28±0.10	...	...	0.90	...	4.00
53.1608238	-27.7753963	21.70±0.06	...	23.44±0.04	22.50±0.02	21.67±0.02	21.42±0.02	22.44±0.06	23.02±0.10	0.64	...	3.00
53.1613579	-27.7957401	22.93±0.10	...	24.48±0.06	24.06±0.04	23.77±0.06	23.54±0.06	24.62±0.25	25.37±0.24	1.00	...	5.67
53.1615295[c]	-27.7676716	22.95±0.10	26.58±0.15	24.96±0.07	24.45±0.04	23.78±0.05	23.70±0.05	21.86±0.00	...	0.69	...	4.00
53.1615944[a]	-27.7922535	20.89±0.02	22.65±0.02	21.81±0.01	21.37±0.01	21.02±0.01	20.77±0.01	21.98±0.04	23.08±0.09	0.42	...	5.33
53.1619873[c]	-27.7925415	21.63±0.04	24.74±0.05	24.91±0.04	24.16±0.02	23.75±0.03	23.71±0.03	21.97±0.03	22.95±0.04	0.25	...	5.00
53.1619949[c]	-27.7739410	21.87±0.06	23.95±0.04	23.58±0.03	22.83±0.02	22.62±0.02	22.53±0.03	22.39±0.04	23.12±0.05	0.26	...	5.67

Table 1—Continued

RA (Deg)	Dec (Deg)	U_{mag}	FUV_{mag}	B_{mag}	V_{mag}	i_{mag}	z_{mag}	GALEX NUV_{mag}	GALEX FUV_{mag}	z_{phot}	z_{spec}	ST
53.1623802[c]	-27.7750893	21.16±0.03	23.66±0.03	22.45±0.02	21.48±0.01	20.97±0.01	20.69±0.01	22.39±0.04	23.12±0.05	0.37	...	3.00
53.1624947	-27.7709045	24.45±0.15	...	25.46±0.11	25.10±0.07	24.61±0.09	24.45±0.09	23.86±0.22	...	1.13	...	6.00
53.1628456[ac]	-27.7672405	21.16±0.03	...	21.17±0.01	20.94±0.01	20.87±0.01	20.84±0.01	21.96±0.03	...	0.05	...	6.00
53.1635971	-27.7935085	21.89±0.07	...	25.17±0.07	25.09±0.05	24.98±0.08	24.47±0.07	...	...	1.54	...	6.00
53.1641121	-27.7873249	23.08±0.05	...	24.95±0.07	24.78±0.05	24.32±0.07	24.00±0.06	...	...	0.75	...	6.00
53.1648941	-27.7787838	23.27±0.12	...	25.31±0.10	25.34±0.08	24.89±0.11	24.63±0.11	...	...	1.26	...	6.00
53.1659012	-27.7815647	22.96±0.05	...	24.67±0.08	24.05±0.04	23.29±0.04	22.79±0.03	...	...	0.95	...	3.33
53.1661797	-27.7875214	21.70±0.05	...	23.02±0.03	22.64±0.02	21.98±0.02	21.41±0.01	...	...	1.04	1.0951	3.33
53.1662140	-27.7939320	21.99±0.10	...	24.56±0.06	24.54±0.04	23.99±0.05	23.63±0.04	23.48±0.24	...	0.71	...	6.00
53.1668854	-27.7976780	22.72±0.06	...	24.37±0.05	24.43±0.04	23.93±0.05	23.75±0.05	24.39±0.23	...	1.18	...	6.00
53.1675873[c]	-27.7925072	23.27±0.54	...	23.76±0.04	23.45±0.02	23.01±0.03	22.72±0.03	23.48±0.24	...	0.71	...	5.67
53.1679382	-27.7781277	23.47±0.12	26.16±0.10	24.86±0.08	24.05±0.03	23.70±0.05	23.63±0.06	...	...	0.26	0.7122	5.33
53.1680222	-27.7896690	22.09±0.07	25.64±0.09	24.12±0.04	23.57±0.02	22.98±0.03	22.90±0.03	24.86±0.14		0.50	...	4.33
53.1680603[c]	-27.8074017	22.91±0.11	25.32±0.08	24.77±0.09	23.97±0.04	23.72±0.06	23.70±0.07	24.35±0.17	25.89±0.27	0.41	...	6.00
53.1681747	-27.8128967	23.16±0.07	...	24.43±0.06	24.06±0.03	23.35±0.04	23.04±0.03	...	...	0.83	...	3.67
53.1699409	-27.7710609	20.59±0.02	...	22.01±0.02	21.18±0.01	20.37±0.01	20.12±0.01	22.94±0.05	25.26±0.20	0.65	...	3.00
53.1703148	-27.7852764	23.07±0.09	25.32±0.07	24.86±0.07	24.15±0.03	23.90±0.04	23.67±0.04	...	...	0.29	0.7122	5.67
53.1704826[b]	-27.7613792	21.58±0.03	...	22.53±0.01	21.84±0.01	21.49±0.01	21.39±0.01	23.16±0.09	23.91±0.09	0.25	...	4.67
53.1705437	-27.8065834	22.75±0.09	...	24.65±0.06	24.67±0.05	24.42±0.07	23.96±0.06	24.74±0.47	...	0.77	1.2441	6.00
53.1706848[bc]	-27.7579365	22.42±0.05	...	24.19±0.08	23.56±0.03	22.98±0.03	22.93±0.04	22.77±0.06	23.16±0.10	0.27	...	5.00
53.1707726	-27.8046780	23.14±0.09	...	24.06±0.05	23.91±0.04	23.71±0.06	23.63±0.07	25.04±0.24	...	1.79	...	6.00
53.1713791[bc]	-27.7574749	20.96±0.02	...	21.69±0.02	21.07±0.01	20.71±0.01	20.63±0.01	22.70±0.04	23.23±0.05	0.25	...	5.33
53.1721077[c]	-27.7969379	23.11±0.13	25.21±0.06	24.58±0.08	23.71±0.03	23.42±0.05	23.32±0.05	22.94±0.05	23.50±0.06	0.19	...	3.33

Table 1—Continued

RA (Deg)	Dec (Deg)	U_{mag}	FUV_{mag}	B_{mag}	V_{mag}	i_{mag}	z_{mag}	GALEX NUV_{mag}	GALEX FUV_{mag}	z_{phot}	z_{spec}	ST
53.1721840	-27.8058681	22.21±0.06	...	23.94±0.06	23.83±0.04	23.71±0.08	23.24±0.06	...	...	0.77	1.3180	6.00
53.1722603	-27.7651482	22.41±0.08	...	23.34±0.04	22.64±0.02	22.01±0.02	21.88±0.02	23.98±0.16	24.65±0.25	0.51	...	3.67
53.1725159[c]	-27.7963371	21.05±0.06	23.66±0.03	23.01±0.03	22.15±0.01	21.85±0.02	21.67±0.02	22.89±0.08	23.27±0.10	0.29	0.3469	3.67
53.1726112	-27.7809887	23.37±0.15	...	24.04±0.06	22.90±0.02	22.05±0.02	21.71±0.01	...	...	0.66	...	2.67
53.1730003	-27.7779026	22.08±0.06	...	24.06±0.04	23.98±0.03	23.53±0.04	23.20±0.04	24.46±0.26	...	0.71	...	6.00
53.1730042[bc]	-27.7590351	20.62±0.02	...	21.51±0.01	20.76±0.01	20.37±0.01	20.26±0.01	22.69±0.06	22.99±0.08	0.26	...	5.00
53.1747513	-27.7992420	19.58±0.03	22.00±0.02	21.14±0.01	20.54±0.01	20.25±0.01	20.14±0.01	22.04±0.03	22.30±0.03	0.26	0.1514	5.67
53.1761894	-27.7961178	21.25±0.06	...	22.87±0.02	22.36±0.01	21.62±0.01	21.23±0.01	24.28±0.18	...	0.86	0.9961	3.67
53.1767311[d]	-27.7996502	22.89±0.12	...	22.53±0.02	20.58±0.00	18.93±0.00	18.32±0.00	...	...	0.70	...	1.33
53.1777191	-27.7869625	22.52±0.07	...	25.15±0.08	25.08±0.07	24.52±0.08	24.41±0.08	...	...	1.12	...	6.00
53.1778793[b]	-27.7577496	23.50±0.12	...	25.02±0.05	25.05±0.05	24.44±0.06	24.27±0.06	...	...	0.91	...	6.00
53.1782227	-27.7830944	21.45±0.05	...	24.03±0.05	23.84±0.03	23.45±0.04	22.92±0.03	...	...	0.77	...	5.67
53.1784172	-27.7682304	21.09±0.05	...	22.39±0.02	21.54±0.01	20.68±0.01	20.39±0.01	23.12±0.07	...	0.72	...	3.00
53.1799660[b]	-27.7573910	23.55±0.13	...	25.28±0.08	24.76±0.05	24.31±0.06	24.33±0.08	...	...	0.68	...	6.00
53.1815453	-27.7879925	22.07±0.04	23.86±0.03	23.94±0.04	23.48±0.02	23.35±0.03	23.44±0.04	23.57±0.14	23.55±0.19	0.07	0.2122	6.00
53.1821976	-27.7939968	23.18±0.09	27.64±0.23	25.70±0.09	25.59±0.06	25.07±0.08	24.93±0.08	...	...	1.13	...	6.00
53.1826210[d]	-27.7681408	19.44±0.00	...	...	...	...	17.45±0.00	...	...	0.30	...	6.00
53.1841164[b]	-27.7559299	22.82±0.13	...	24.89±0.06	24.73±0.05	24.41±0.07	24.33±0.08	...	...	1.89	...	6.00
53.1841660	-27.7926407	21.36±0.02	25.92±0.13	22.90±0.02	22.33±0.01	21.65±0.01	21.44±0.01	...	...	0.69	0.7372	3.67
53.1841698	-27.7915535	23.38±0.10	...	24.95±0.14	24.48±0.07	23.77±0.07	23.36±0.06	...	...	1.45	...	3.00
53.1855202[b]	-27.7554283	22.01±0.07	...	23.96±0.03	23.07±0.01	22.52±0.02	22.36±0.02	...	...	0.43	0.5328	3.33
53.1869583[c]	-27.7910004	19.03±0.01	21.67±0.01	20.21±0.01	19.19±0.00	18.65±0.00	18.44±0.00	21.32±0.02	21.89±0.02	0.23	...	2.33
53.1877899[c]	-27.7940979	19.83±0.02	22.23±0.02	21.49±0.01	20.68±0.01	20.45±0.01	20.23±0.01	21.95±0.02	22.49±0.03	0.27	0.3446	3.67

Table 1—Continued

RA (Deg)	Dec (Deg)	U_{mag}	FUV_{mag}	B_{mag}	V_{mag}	i_{mag}	z_{mag}	GALEX NUV_{mag}	GALEX FUV_{mag}	z_{phot}	z_{spec}	ST
53.1879463[b]	-27.7615261	21.55±0.06	...	21.50±0.01	20.61±0.01	20.22±0.01	20.05±0.01	23.59±0.11	24.47±0.21	0.22	...	3.33
53.1879768[ac]	-27.7900066	21.10±0.03	24.86±0.06	22.69±0.02	21.53±0.01	20.79±0.01	20.39±0.01	21.32±0.02	21.89±0.02	0.51	0.4357	2.33
53.1898384[b]	-27.7588539	20.64±0.03	...	21.84±0.01	21.41±0.01	21.17±0.01	21.17±0.01	22.43±0.04	22.65±0.03	0.24	...	6.00
53.1901550[b]	-27.7651958	20.49±0.06	...	22.01±0.02	20.95±0.01	20.52±0.01	20.29±0.01	22.82±0.07	23.69±0.13	0.36	...	3.00

[a]X-ray source (Koekemoer et al. 2004)

[b]Source is outside the UDF footprint

[c]Confusion in GALEX image

[d]Star